Synthetic transfer zone characterization using seismic attributes: An example from the Parihaka fault system in the Taranaki Basin, New Zealand

Pierre Karam[1], Shankar Mitra[1], Kurt Marfurt[1], and Brett M. Carpenter[1]

Abstract

Synthetic transfer zones develop between fault segments that dip in the same direction, with relay ramps connecting the fault blocks separated by the different fault segments. The characteristics of the transfer zones are controlled by the lithology, deformation conditions, and strain magnitude. The Parihaka fault is a northeast–southwest-trending set of three major en echelon faults connected by relay ramps in the Taranaki Basin, New Zealand. The structure in the basin is defined by extension during two episodes of deformation between the late Cretaceous and Paleocene and between the late Miocene and recent. To better understand the evolution of a synthetic transfer zone, we studied the geometry and secondary faulting between the individual fault segments in the Parihaka fault system using structural interpretation of 3D seismic data and seismic attributes. This interpretation allows for a unique application of seismic attributes to better study transfer zones. Seismic attributes, such as coherence, dip, and curvature, are effective tools used to understand the detailed geometry and variation in displacement on the individual faults, the nature of secondary faulting along the transfer zones, and the relationship between the faults and drape folds. The seismic characterization of the fault system of Miocene to Pliocene age horizons highlights variations in the degree of faulting, deformation, and growth mechanism associated with different stages of transfer zone development. The coherence, dip, and curvature attributes indicate a direct correlation with structural parameters such as deformation, folding, and breaching of relay ramps. All three attributes enhance the visualization of the major and associated secondary faults and better constrain their tectonic history. The observed correlation between the seismic attributes and structural characteristics of transfer zones can significantly improve the structural interpretation and exploration workflow.

Introduction

Transfer zones are ramps that connect two faults (the upthrown of one to the downthrown of another) by transferring displacement from one fault to another. They have been extensively studied to better understand the transfer of fault slip with consideration of their importance for fluid migration and fracture distribution at different scales (e.g., Morley et al., 1990; Nicol et al., 2007; Ferrill and Morris, 2008). There are multiple transfer zone types, depending on the relative dip directions of adjacent faults and the distribution of slip along individual faults. Supplemental information can be accessed through the following link: Figure S1 shows the classification of transfer zones depending on how faults are dipping and their relative positions. These include divergent, convergent, synthetic, collateral, and colinear transfer zones (Morley et al., 1990). Convergent and divergent zones are defined by faults dipping in different directions either toward each other (convergent) or away from each other (divergent). Synthetic transfer zones consist of faults that dip in the same direction and are separated by strike or relay ramps. The relay ramps transfer displacement between the faults (e.g., Morley et al., 1990). Approaching faults initially terminate along trend, commonly branching into several smaller fault splays. As the fault-related extension increases, a transfer fault can connect some of the smaller initial faults and result in fully detached blocks (Larsen, 1988). Relay ramps play an important role in defining traps, reservoirs, and migration conduits or barriers for hydrocarbon exploration.

Peacock and Sanderson's work published between 1991 and 1995 is a series of publications that investigate the relationship among displacement variations along faults, fault segment linkage, strain estimation, and relay ramp geometries within a normal or strike-slip system. Displacement at a transfer zone is seen to be reduced caused by folding or tilting of beds within

[1]University of Oklahoma, School of Geosciences, Norman, Oklahoma 73019, USA. E-mail: pierre.j.karam-1@ou.edu (corresponding author); smitra@ou.edu; kmarfurt@ou.edu; brett.carpenter@ou.edu.

Manuscript received by the Editor 14 July 2020; revised manuscript received 24 January 2021; published ahead of production 29 March 2021; published online 15 June 2021. This paper appears in *Interpretation*, Vol. 9, No. 3 (August 2021); p. T653–T665, 15 FIGS.
http://dx.doi.org/10.1190/INT-2020-0138.1.

DOI:10.1190/INT-2020-0138.1

the relay ramp while maintaining a constant ramp rotation (Peacock and Sanderson, 1991, 1993, 1995). This variation in displacement at relay ramps causes a variation in the *d-x* (distance versus displacement) plots along the geometry of the structure. Hence, Peacock and Sanderson (1991) define four stages of relay ramp development based on the displacement profiles of the two main faults. This definition was later revised and published in 1994 with a more detailed description of relay ramp growth for normal faulting (supplemental information can be accessed through the following link: Figure S2). Those four evolutionary stages involve (1) fault initiation, (2) fault propagation, (3) relay ramp breaking and development of a connecting fault, and finally (4) the complete faulting and breaking of the ramp with multiple composite along-strike faults.

As the displacement increases, breaching of the transfer zone occurs. Fossen and Rotevatn (2016) define fault linkage as the result of one of two end member scenarios, either a tip propagation model of randomly distributed small faults or through coherent growth caused by a preexisting buried fault being reactivated. The growth of faults is controlled by different parameters such as fault population and distribution, stress orientation and perturbation, boundary conditions such as weak fabrics or preexisting smaller faults, and reactivated basement faults. Because displacement is being transferred from one fault to another, the spacing of the two faults impacts the length of the ramp. Depending on the sedimentary layer, as faulting continues, breaching within the relay structure may occur together with lengthening and bending of beds causing fracturing and faulting of the ramp. This fracturing is quite important for vertical and lateral fluid movement, migration, or entrapment. Observations from outcrops can provide limited information on those characteristics. Studies in quarries in South Texas by Ferrill and Morris (2008) enabled an understanding of the deformation mechanics and transfer zone characteristics for beds with different brittleness.

Conneally et al. (2014) further modify the relay zone evolution model by determining the geometry and kinematic history of two relay zones from the South China Sea. They determine that kinematic analysis using 3D seismic interpretation showed that the mechanism of breached zones development might have included the formation of a "through-going" fault followed by the development of a splay within the breached zone. This can be seen by the rotation of the ramp, which occurred after the faulting and prior to the formation of splay geometries. The data that Conneally et al. (2014) use included an upper and a lower relay zone that were vertically separated by 100 m of sediments, thus suggesting causality between the two structures. A possible explanation indicates that the lower relay zone might have been "triggered" by the development of the upper ramp due to the complex inherited geometry.

The availability of 3D seismic data enables a more detailed understanding of relay ramp growth. Considering the limited work in the literature done on the application of seismic attributes to structural properties (Lohr et al., 2008; Iacopini et al., 2016), this paper presents an application of attributes to better characterize transfer zones. In this paper, we investigate the geometry and development of relay ramps in the Parihaka fault system in the northern Taranaki Basin, New Zealand. The Parihaka fault system is defined by a series of en echelon faults forming a synthetic transfer zone. Major and secondary faults and the associated relay ramps are generally well imaged in 3D seismic amplitude data. We first use a traditional 3D seismic interpretation workflow to study the geometry of the synthetic transfer zone and the related relay ramps. Displacement patterns of individual faults and at relay ramps are mapped for different units to understand the evolution of the transfer zones. We then use three seismic attributes, namely, coherence, curvature, and dip and azimuth, to study the deformation patterns on the major faults as well as the related folds and secondary faults. Our results provide a better understanding of the deformation patterns within the transfer zone and serve as a test for the use of attribute analysis in transfer zone characterization.

Taranaki Basin setting

The Taranaki Basin is a Cretaceous sedimentary basin encompassing approximately 100,000 km^2 located off the western coast of New Zealand. It formed as an active volcanic back-arc rift basin (Giba et al., 2010) during the subduction of the Pacific plate beneath the Australian plate (Haque et al., 2016; Rajabi et al., 2016). The formation of the basin is defined by three stages: an extensional phase that occurred from the late Cretaceous to Paleocene time characterized by the formation of graben and horst structures along a north–south normal faulting system (King and Thrasher, 1996; Giba et al., 2010), a shortening phase primarily confined to the southern part of the basin caused by the subduction of the Pacific plate, and another extensional phase starting in the late Miocene occurring in different locations (King and Thrasher, 1996; King, 2000). Subsidence increased significantly between 30 and 25 Ma (King and Thrasher, 1996) induced by mantle convection as subduction continued on the eastern side (Stern and Holt, 1994). Gradual southward and eastward migration of volcanism and faulting is evident at approximately 18 Ma due to the rollback of the Pacific plate (King, 2000; Nicol et al., 2007; Giba et al., 2010).

The sedimentation rate within the basin is seen to be higher than the fault displacement rate, resulting in the preservation of units in both blocks and thickness increases across the faults into the downthrown blocks. Sediments were deposited in the basin in large volumes due to the erosion of areas with positive relief (King, 2000). Within the South Taranaki Basin, the vertical displacement rate was the largest during the late Cretaceous (Reilly et al., 2015). The sedimentary record from the northern Taranaki Basin indicates significant

DOI:10.1190/INT-2020-0138.1

displacement approximately 29 Ma seen by the activation of the Manganui fault (Tripathi and Kamp, 2008).

The Parihaka fault, our focus, is located in the northern central part of the Taranaki Basin (Figure 1), and it underwent normal faulting. The fault system is approximately 50 km long and comprises five segments forming an en echelon system striking north–south to northeast–southwest (Giba et al., 2012). According to Giba et al. (2012), the fault has up to 1.8 km in vertical displacement with the maximum displacement shifting to the north during Plio-Pleistocene time, while becoming almost inactive in the southern part. The minimum displacement on the faults coincides with the locations of the relay ramps.

Reservoir stratigraphy

Targeted formations in the basin consist mainly of the Rangitikei group (mainly the Giant Forest and Matemateonga), the Wai-ti group (including the Urenui, Mt Messenger, Mohakatino, and Moki), and down to the Nigatoro group. According to Tripathi and Kamp (2008), the Rangitikei group is a late Pliocene formation deposited mainly in a regressive system track with thinly deposited transgressive beds. Sediments are characterized by alteration of 4–5 m thick sandstone layers along with thick mudstone intervals as part of a submarine fan system. The Matemateonga sequence that started depositing during the late Miocene through the early Pliocene consists of predominately sandstone interbedded with siltstones deposited in a shelf to marine environment (according to a report acquired from the New Zealand Ministry of Economic Development prepared in 2009, report PR 1745).

Based on the available New Zealand government reports for exploration in the Taranaki Basin, the Wai-ti group is defined to be Miocene in age and spans approximately 20 million years consisting of primary exploration targets. The Urenui Formation within the Wai-ti group is mainly a siltstone and mudstone interval comprising thick claystones that are eroded in some areas with channels (report PR 1745). Urenui is a continuous formation that can easily be picked on seismic lines. The Mt. Messenger Formation is one of the targeted reservoirs consisting of fine to medium coarse sandstones with minor interbedded mudstones. The base of Mt. Messenger is defined by a sonic marker caused by the cementation of planktic foraminifers (Tripathi and Kamp, 2008). The underlying formation is the Mohakatino lower slope formation redeposited by volcanic highs during the reactivation of the Taranaki Graben. The unit consists mainly of reworked detritus volcanic deposits, highly heterogeneous siltstones and mudstones, noncontinuous sandstone reservoirs, highly faulted and fractures intervals, and rich in swelling clays.

Other units form the Wai-ti sequence including the Awakau formation (interbedded sandstone, siltstone, and shale), the Manganui formation (predominately mudstone deposited in a deepwater setting), and down to the Moki formation (report PR 1745). The Moki formation mainly consists of deepwater turbidites with sand channels clearly seen on the seismic amplitude and seen to be controlled by faulting.

Data and interpretation methods

A 3D poststack time-migrated seismic volume for the area west of New Zealand covers a large area of the Parihaka fault. The seismic volume was provided through the SEG data storage facility and covers most of the three en echelon faults connected by relay ramps. Supplemental information can be accessed through the following link: Table S1 summarizes the main details of the seismic volume. In general, the seismic quality is very good mainly in the section covering the faulting system. Despite the seismic acquisition footprints in the shallower part, the footprint contaminates the survey in the shallower section, but it does not significantly inhibit a good interpretation of faulting, folding, and stratigraphic features. The seismic volume was reprocessed in 2012 for the purpose of improving the Miocene target, to better image the deeper targets west of the Cape Egmont fault, the top of the basement, the Cretaceous geology, the shallow biogenic gases in the north, and the geohazards. A full summary of the processing report containing full details on the workflow and algorithms was acquired from the New Zealand Ministry of Economic Development (report PR 4582).

Well data including logs, check shots, core descriptions, mud log reports, drilling reports, geochemistry, and other data were available for three wells in the area. Only one of the wells (Arawa 1) available falls within the 3D seismic volume that covers the interpreted intervals. The well data were used to correlate key units in the seismic data. Check-shot data were used to build a velocity model to allow the depth conversion of the interpreted horizons. Likewise, the biostratigraphy data from the Arawa 1 well were then used to estimate the age of those interpreted horizons and thus were able to estimate the timing of the structural movements.

Structural analysis of the synthetic transfer zone consisted of two main components. The first component consisted of a traditional approach of analyzing the transfer system including a 3D analysis of the fault zones, the variation of slip on both individual faults and along relay ramps connecting the individual faults. Figure 1 shows the three main faults interpreted within Pleistocene to Pliocene units. Figure 2 represents a map view of a time slice at t = 860 ms through a coherence volume. The coherence displayed is a measure of how coherent the seismic response is thus allowing us to pick and determine areas of variability, which then reflects the presence of discontinuity. The darker continuous colors, trending mainly north–south, are the major en echelon faults in the area defined in this paper as fault A, fault B, and fault C. Ramp 1 is defined as the ramp connecting faults A and B, whereas ramp 2 is defined as the ramp connecting faults C and D. Note the

DOI:10.1190/INT-2020-0138.1

location of the Arawa 1 well on the upthrown side of fault A in close proximity to ramp 1.

The second component consisted of seismic attributes analyses to refine the fault interpretation and the related deformation in the vicinity of the relay ramps. This analysis included the use of variance (coherence), maximum positive and negative curvature, seismic dip, and seismic azimuth. We conducted our analyses using time slices as well as horizon slices through the attribute volumes. In contrast to time slices through the original seismic amplitude, time slices through the dip, curvature, and coherence volumes are relatively insensitive to the seismic wavelet and are thus quite easy to interpret on time slices.

Fault characterization

A time-depth conversion based on one well (Arawa 1) was used to better interpret the structure and related faults in depth. The data show an overall consistent increase in velocity with depth. The model was separated into three velocity trends to accommodate for velocity changes with depth and a more accurate depth conversion. Supplemental information can be accessed through the following link: Figure S3 shows the velocity data from the Arawa 1 well plotted with depth for the check-shot data. Different colors represent different defined trends in the velocity model that was adopted during the depth conversion. Depth-converted horizons allow for appropriate calculations of fault displacement and the associated throw. However, horizon names were used for fault characterization and structural analysis due to the large displacement and associated folding seen on those faults, which makes using only depth information hard to understand.

Examining Figure 3, horizon 1 shows almost no displacement across the fault, with the displacement increasing to a maximum with horizon 11. The approximate age of the horizons was determined using biomarker data provided by the New Zealand Ministry of Economic Development for the Arawa 1 well, and it is shown in the supplemental information that can be accessed through the following link: Table S2. The downthrown units associated with extension show growth or an increase in thickness compared with the upthrown units. Similar observations on other faults indicate that the region was structurally active as a part of the extensional system during the deposition of those units. Supplemental information can be accessed through the following link: Figure S4 shows the variation in displacement along the length of fault B. For each unit, the displacement decreases from a maximum in the center of the fault to a minimum at the fault tips, suggesting an increase in fault displacement with the increasing lateral fault propagation. It also shows the

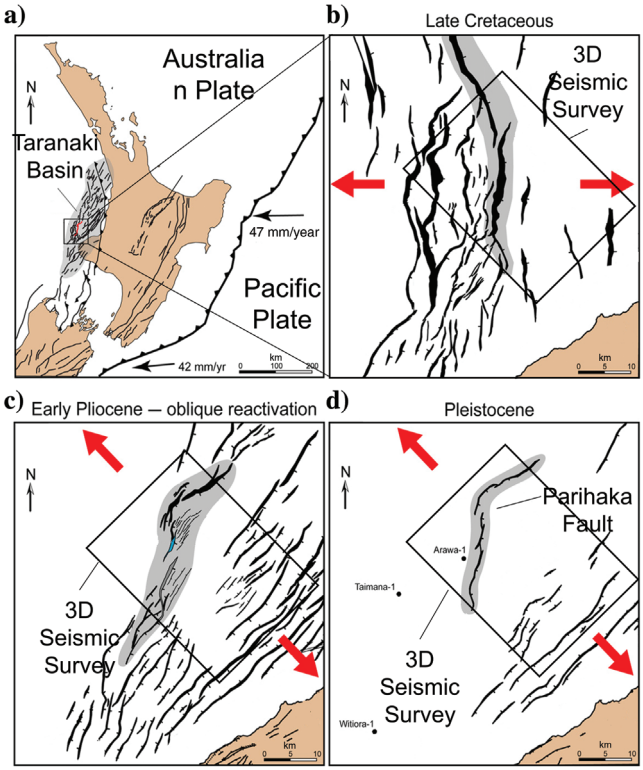

Figure 1. Plate boundary setting of the North Island of New Zealand. (a) Regional setting during the late Cretaceous, (b) magnified view at the region during the late Cretaceous, (c) Parihaka fault during the early Pliocene, and (d) Parihaka fault during the Pleistocene (edited from Giba et al., 2012) (the red arrows indicate the approximate extension directions).

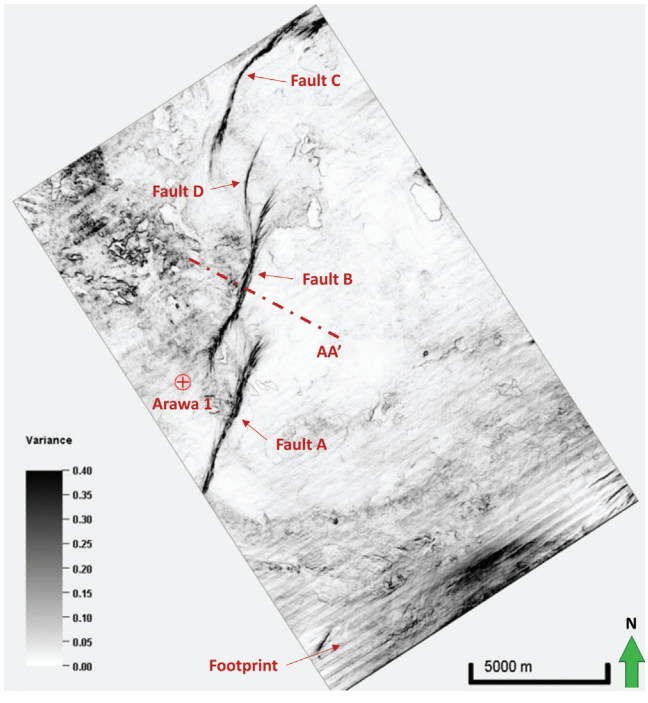

Figure 2. Time slice at t = 860 ms through a coherence volume showing the location of the main faults in the area (A, B, C, and D), the Arawa 1 well, and the location of cross-section AA′. The northeast-trending acquisition footprint corresponds to the sail line of seismic acquisition. High-coherence elliptical features are shallow gas accumulations forming bright spots, which can be seen in the following figure.

DOI:10.1190/INT-2020-0138.1

progressive increase in the maximum displacement of each unit with depth implying a progressive increase in growth. The increase in separation of the curves between horizons 8 and 10 suggests a rapid increase in growth during the deposition of the units.

By measuring the thickness change at the maximum displacement locations across the three main faults A, B, and C, we compute the growth index, defined as the ratio of the hanging wall to footwall thickness (Thorsen, 1963), to assess the relative growth associated with each horizon for each of the three main (faults A, B, and C) faults. Figure 4 summarizes the findings for the main faults at all 11 horizons. The growth index increases from horizon 1, showing lower growth, to horizon 7, which has higher growth. Horizons 1–5 are Pleistocene, whereas horizons 6–11 are Pliocene in age. Minor changes in relative growth are seen for the different faults for these horizons. During deposition of geologic units underlying horizons 8–10, the growth index for the different faults varies considerably suggesting changes in extension along the fault system. Furthermore, whereas the growth index is highest for fault A for units 8 and 9, it is highest for fault C for units 9 and 10, suggesting the transfer of displacement along the trend from fault A to fault C during this time.

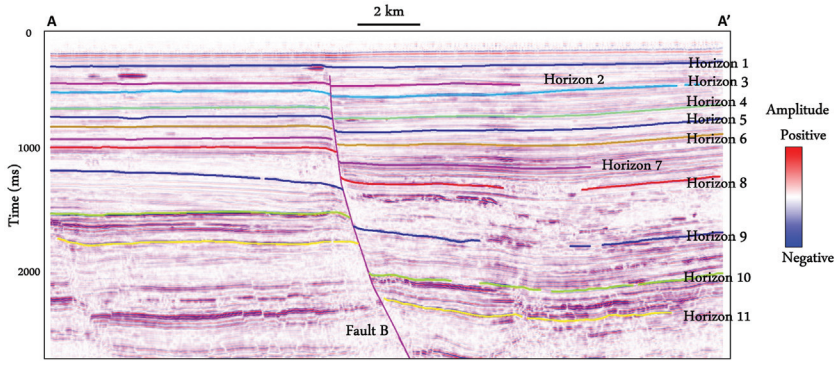

Figure 3. Cross-section AA′ showing all 11 horizons interpreted to assess the relay ramp formation.

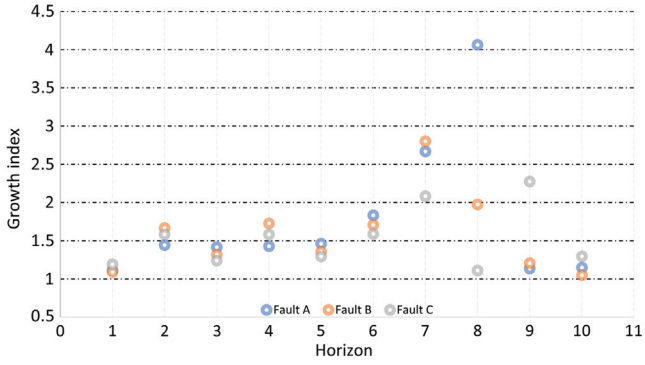

Figure 4. Growth index (ratio of downthrow to upthrown thickness) for all three faults.

Another key parameter analyzed was the relationship between the fault length and displacement during propagation of each major fault through the major mapped horizons. The fault length was measured at each horizon and plotted against displacement for all four faults shown in Figure 2. Figure 5 shows the fault length versus displacement for every horizon. Shallower horizons (starting with horizon 1) show shorter fault lengths compared with the deeper horizons, due to the progressive increase of the fault length with the increasing displacement. However, the rate of change of the fault displacement shows three distinct trends: (1) an "early" episode of rapid fault length increase characterized with little displacement, (2) a "second" episode characterized by a rapid increase in fault displacement associated with little or a small increase in the fault length, and (3) a final episode of fault length increase with little fault displacement. These changes in the rates of displacement with fault length can be attributed to two main factors: (1) the general change in fault displacement with length during the propagation of the faults as discussed by Rotevatn et al. (2018) and (2) changes in the rates of propagation caused by variations in the mechanical properties of the individual units. Rotevatn et al. (2018) discuss two fault growth models consisting of (1) a propagation model or an isolated fault model in which the fault displacement is positively related to the fault length and (2) a constant-length model in which the faults establish most of their length early on in their history and displacement accumulates without major increase in fault length. The plot of the four faults (Figure 5) can be explained due to rapid fault growth in the early stages of evolution (Rotevatn et al., 2018) and also to changes in fault propagation rates due to variations in the mechanical properties of the units.

Relay ramp characterization

We now examine the variation in displacement along the ramps and transfer

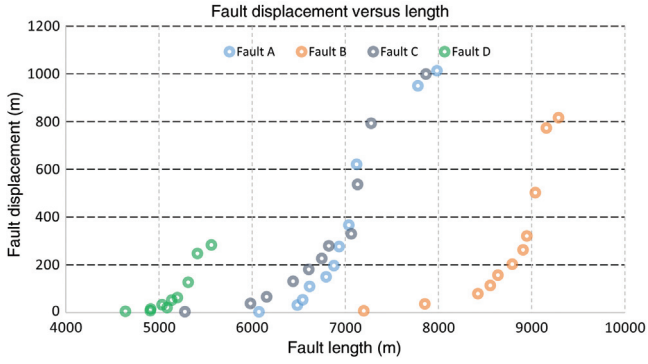

Figure 5. Fault length plotted versus fault displacement of all horizons for the four major faults.

DOI:10.1190/INT-2020-0138.1

zones for the different horizons. Figure 6 shows a cross section along the faults from the southwest to the northeast in the area. The cumulative displacement at any point along the cross section for all interpreted faults is plotted. The plot shows the displacement variations for four representative horizons (horizons 4, 8, 10, and 11). For each major fault and the related secondary faults, the displacement is at its maximum in the center of the fault and decreases to a minimum along the transfer zones. There is an overall decrease in the fault displacement to the northeast for the deeper horizons 10 and 11. For horizon 8, the decrease in displacement to the northeast is smaller than that for the deeper horizons. The displacement pattern reverses for the shallowest mapped horizon (horizon 4) for which there is a slight increase in displacement to the northeast. This pattern may be associated with the change in the relative extension direction during the Pliocene. Similar observations regarding the variation in displacement were also made by Giba et al. (2012) for this area and by Lohr et al. (2008) in the northwest German Basin.

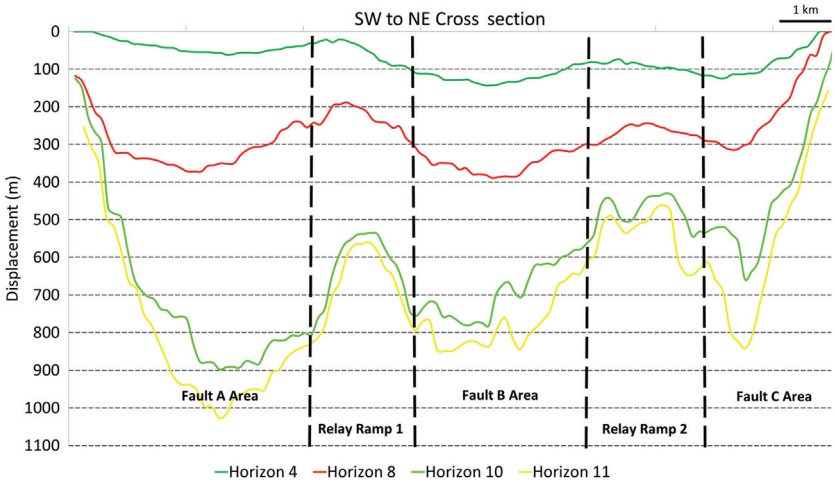

Figure 6. Cross section along the main faults extending from the southwest to the northeast direction showing displacement for four main horizons.

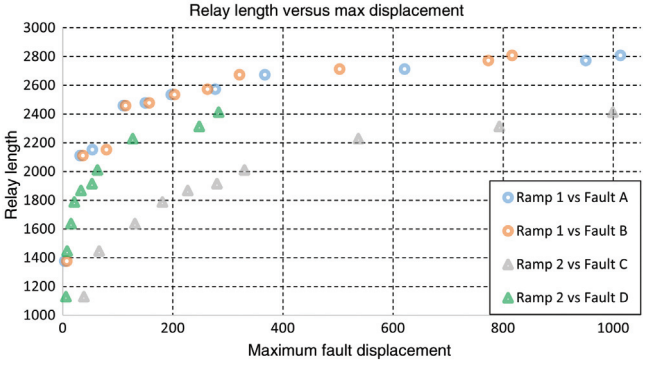

Figure 7. Measured ramp length plotted against the maximum displacement associated with the related faults.

Relay ramps can be seen on time slices, particularly for shallower horizons (from horizon 1 to horizon 7). With an increase in displacement, relay ramps are often cut by small faults, which connect the major faults, thus making it more difficult to examine displacement transfer. Ramps connecting the different faults were examined by recording the ramp length and width and plotting them against the maximum displacement observed on both faults defining the ramp. Figure 7 shows the relay ramp length increasing with the increase of displacement at every horizon for both connected faults. For faults A and B, the maximum displacement is similar causing almost identical data points relating the displacement to the ramp length for ramp 1, whereas fault C shows slightly smaller fault displacements and related ramp lengths for ramp 2. Fault D is a much smaller secondary fault associated with fault B and shows the smallest fault displacements.

The relationship between the displacements and lengths of ramps 1 and 2 follow a logarithmic pattern, characterized by a sharp increase in the ramp length, so that most (70%–80%) of the length is attained with little displacement (less than 25% extension), followed by a flatter curve associated with small additional increases in the ramp length with additional extension. Similar to the fault growth shown in Figure 5, the logarithmic pattern in the relay ramp length increase is associated with a similar logarithmic increase in the fault length (Walsh and Watterson, 1988). Because the ramp length is related to the length of the fault, the flatter curve supports that the fault propagation occurs at a higher rate in the early stages relative to the fault displacement. The ramp width (shown in the supplemental information that can be accessed through the following link: Figure S5), is independent of the increase of displacement for both ramps.

The ramp width is defined by the initial location of the faults relative to each other, and it is possibly controlled by the location of preexisting basement faults. The ramps quickly extend in length, as adjacent faults transition from approaching to overlapping patterns, eventually curving and connecting with each other or terminating against each other. The growth history of the faults is associated with a significant gain in fault length in the initial stages and then a smaller gain in length with the increase in displacement. Ramps transfer the additional displacement from one fault to the other without significant additional fault growth.

Seismic attribute analyses

Seismic attribute analysis was used to understand the detailed geometry of faults and related deformation within the transfer zones. Different seismic attributes

DOI:10.1190/INT-2020-0138.1

can be used to help structural interpretation and to better understand fault geometries and displacements. The attributes provide a better visualization of the faults and, in some instances, reduced ambiguity in fault location than the original seismic amplitude volume. We summarize the main attributes used in our analysis, including coherence, volumetric dip magnitude and dip azimuth, and most-positive and most-negative curvature.

The dip magnitude and dip azimuth volumes define the orientation of a plane that best presents the seismic reflection pattern at each voxel in the data volume. For time-migrated data, the dip magnitude is measured in ms/m, which through the use of a simple velocity model can be converted to degrees. Using 3D visualization and appropriate color bars, horizon slices and time slices through the vector dip provide easy to understand images of structural deformation.

Coherence measures the similarity of the waveform within a small 3D window (Bahorich and Farmer, 1995), providing better visualization of discontinuities in the data such as faults, large fractures, and stratigraphic edges (such as the turbidites). By using a small 3D analysis window, coherence provides excellent images of faults on time slices, whereas faults parallel to the bed strike are easily confused with stratigraphic changes (Bahorich and Farmer, 1995). An eigenstructure coherence algorithm can be applied to produce better results and improve image quality to account for noise and low signal-to-noise ratios (Gersztenkorn and Marfurt, 1999).

Curvature is a second-order derivative of the time structure or the first derivative of the vector dip. Whereas the vector dip can be expressed by a single vector, curvature requires two vectors — the value and the strike of the most-positive and most-negative curvatures. Used together, these two vectors provide a representation of the domes, ridges, saddles, valley, bowls, and planes within the data volume (Roberts, 2001). Curvature anomalies tend to bracket, rather than align with, coherence anomalies. For normal faults, there is usually a positive curvature anomaly on the footwall side of the fault and a negative curvature anomaly on the hanging wall side of fault. In our present study, this attribute can be used to identify folding of different wavelengths in addition to the faults. Overlaying the most-positive and most-negative curvature on a time slice enables the

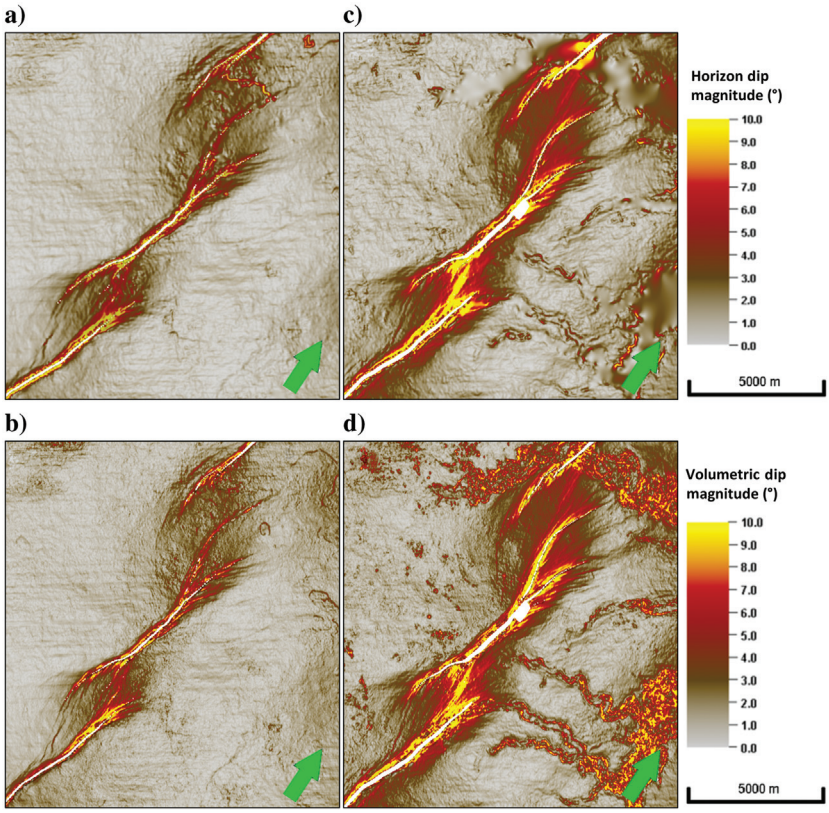

Figure 8. Comparison between the dip magnitude computed from an interpreted horizon and a horizon slice through a volumetric dip computation for (a and b) horizon 6 and (c and d) horizon 8, respectively (the mapping grid size is 100 × 100 m). Note the improved resolution of the three turbidite channels in (d) versus (c). The subtle left-to-right corrugations are due to the acquisition footprint.

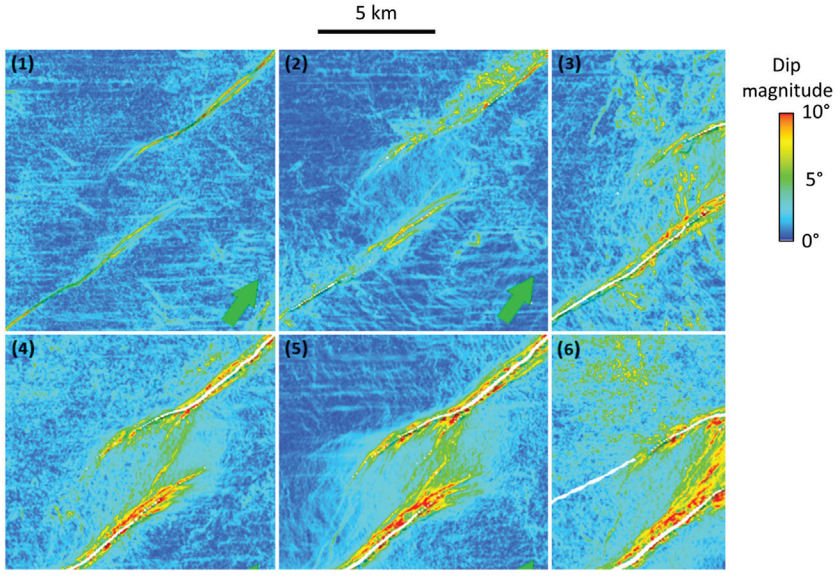

Figure 9. Horizon slices through the dip magnitude volume for horizons 1–6 for ramp 1.

visualization of folds, faults, and other structural features. The most-positive and -negative curvatures are always orthogonal and show anomalies along the fold crests or troughs (Marfurt, 2010).

Applications of seismic attributes

Horizon-based versus volumetric dip calculations

Seismic dip (Marfurt, 2006) was derived and mapped for all interpreted horizons. In addition, dip was calculated by structural modeling and depth conversion for all interpreted horizons. Figure 8 presents a comparison between the seismic dip and structural dip for various horizons for the two ramps. As shown in Figure 8, the derived seismic dip can be very close to the actual structural dip calculated for the interpreted horizons. Along relay ramps, the dip of the beds changes along the ramp from the upthrown side of one fault to the downthrown side. Bed dips increase from subhorizontal to more steeply dipping to subhorizontal again. The dip change relates to displacement transfer along the ramp. To examine the relation of bed dipping (tilting) with fault development along relay ramps, multiple images of dip change for different horizons were examined. Considering the similarity of the seismic dip and structural dip along the ramps, Figure 9 shows seismic dip attributes along the ramps. Because the beds rotate by 5° or 6°, the ramps develop smaller faults to account for the additional tilting on the ramps. This angle of breaching development within the transfer zone is much lower that what was suggested by Fossen and Rotevatn (2016) of 10°–15°. The actual dip angle for the fault initiation can be formation-specific and depends on the lithologic characteristics. For ramp 2, the breaching occurs at a deeper formation and the same horizon 5 that is faulted at ramp 1 does not show any faulting at ramp 2 (Figure 10). Breaching is initiated between horizons 6 and 7. Similar to ramp 1 that breaching is associated with a dipping angle of almost 6°. The deeper breaching is because fault D does not have as much displacement as faults A, B, and C.

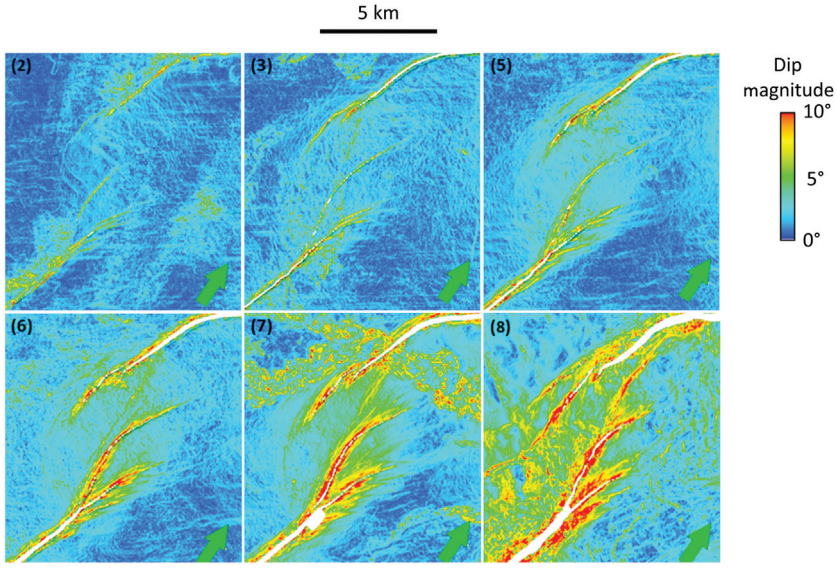

Figure 10. Horizon slices through the dip magnitude volume for horizons 2–8 for ramp 2.

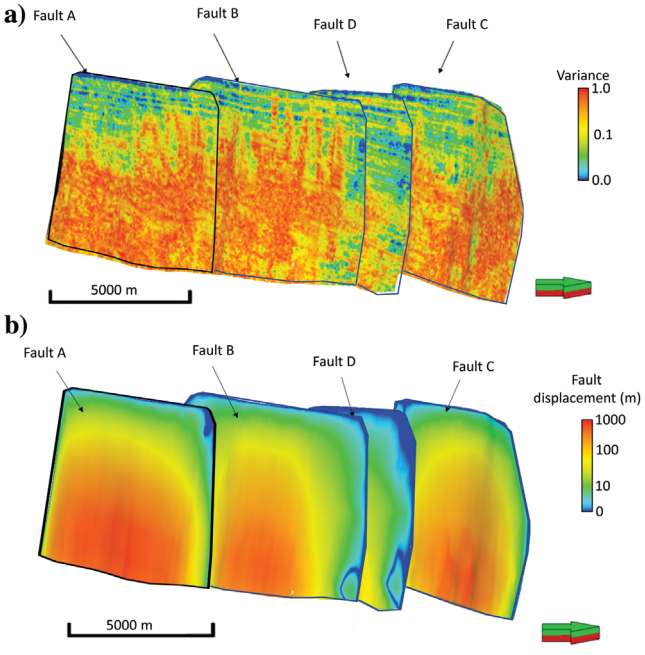

Figure 11. (a) Mapped variance onto the fault planes with red indicating an increase in variance from horizons 1 to 11 and (b) calculated heave using depth-converted seismic data showing an increase of displacement toward the bottom center part of the faults (four times vertically exaggerated).

Coherence or variance

Coherence is an effective tool for visualizing structural changes in seismic data. Although eigenstructure coherence shows the stratigraphic and hydrocarbon edges better, in this application, variance (1 semblance) shows improved delineations about the fault tips where there is no change in waveform shape, but only a change in amplitude. Figure 11a shows fault planes A, B, C, and D with mapped variance volume, corresponding to an averaging of a 50 ms window. The changes in color represent the changes in variance along the fault such that red colors indicate a higher variance (less coherent reflectors). A variance of 0 indicates coherent reflectors with no faulting, whereas a variance of 1 indicates a totally incoherent seismic signal within the analysis window. The observed changes follow the changes in displacement on the faults. Supplemental information can be accessed through the following link: Figure S7 shows the increase in displacement toward the bottom-center part of the faults, which is consistent with the overall increase

in variance. Figure 11b shows the changes in heave measurements along those same faults, showing a better match with the variance derived from seismic. Along the plane of maximum displacement at every fault location, the average variance was measured for every interpreted horizon and plotted with maximum displacement in Figure 12. The increase of displacement is consistent with an increase in variance observed particularly for variance of less than 0.5. Therefore, variance can be used as a direct measure of fault displacement or fault heave for seismic data.

Variance (similar to coherence) below a certain threshold can also to study the nature of secondary faulting. This is useful for predicting and mapping the distribution of smaller faults in a faulted zone. Figure 13 shows examples of variance at representative horizons, within the ramps area, close to the faults, highlighting additional possible smaller faulting. The variance indicates a change in color at the tip of the faults and splaying of the faults into smaller subfaults or splays. Assuming that the variance (or coherence) is a measure of displacement, location of displacement within the relay ramp can be determined. Those are the locations of the initial breaching as well as locations where possible fault displacement is occurring.

Seismic curvature

Curvature measures the variation of a local surface from a plane. In terms of fault tectonics, curvature is a good proxy in measuring strain. Figure 14 shows a horizon slice along horizon 8 through the corendered most-positive and most-negative curvature and a vertical slice through the corendered most-positive and most-negative curvature and the seismic amplitude volumes. Note that the footwall side of the fault exhibits a positive-curvature anomaly (in red) and the hanging wall exhibits a negative-curvature anomaly (in blue) common to many, if not most, normal fault geometries. Note on the horizon slice that the fault discontinuity does not line up with the curvature anomalies, indicating a lateral error in the fault picks.

Figure 15 shows a suite of nine horizon slices through the corendered most-positive and -negative curvature volumes. As in the previous figure, the curvature attributes near the fault zone show positive curvature on the upthrown block and negative curvature on the downthrown block related to folding of the beds. Beds on the upthrown block rotate into the fault forming anticlines, whereas on the downthrown side, beds rotate up to the fault (up to 10° or more dip), forming a syncline. Deeper formations (horizons 8–11) tend to have more complex attributes caused by the longer structural history and additional tectonic events that they underwent. In addition to these larger scale features, the curvature also shows a very sharp increase over a short distance near the fault, attributed directly to the faulting.

The degree of curvature can be seen to correlate with the amount of displacement on the faults. As the displacement increases, the amount of curvature increases indicating increased bed rotation. By examining the cross section shown in Figure 3, the overall geometry of the beds outside the fault zones is seen to be flat, with consistent rotation near the fault. The magnitude of rotation and the width of the folded zone are associated with the displacement as well as the lithology.

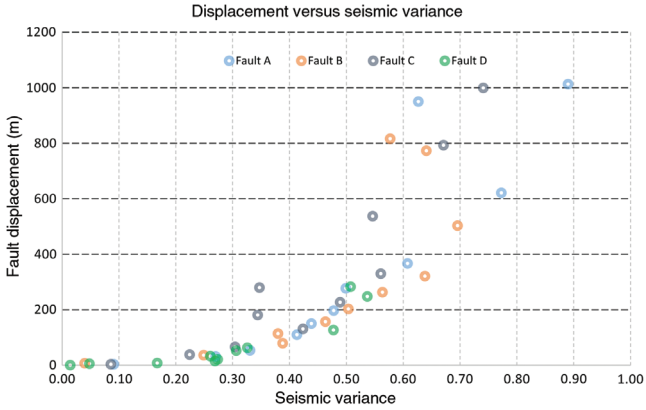

Figure 12. Maximum displacement seen for every fault at every horizon plotted against the average variance measured from the mapped seismic attributes.

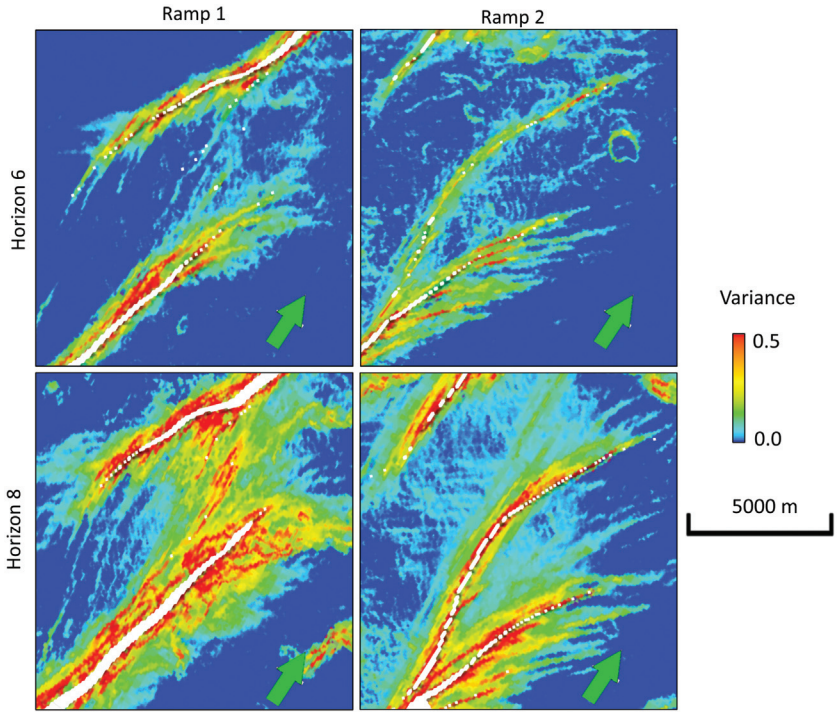

Figure 13. Magnified images of horizon slices along horizons 6 and 8 through the variance volume showing small subseismic faulting along ramps 1 and 2.

DOI:10.1190/INT-2020-0138.1

Traditional models of transfer zones (Morley et al., 1990) show only broad rollover folding of beds related to the changes in fault dip, but no additional folding in the immediate vicinity of the fault. However, experimental studies (Paul and Mitra, 2013) suggest that in many instances, additional extensional fault-propagation or drape folding occurs in the vicinity of the faults, altering the geometry of the transfer zone. Drape folds, accompanied by drag folding, produce the curvature changes described above for the Parihaka fault system. Therefore, the broader curvature changes directly record drape folding, whereas the sharp changes reflect the effects of the faulting. The presence of the drape is also supported by the cross sections through the traditional amplitude data (Figure 3).

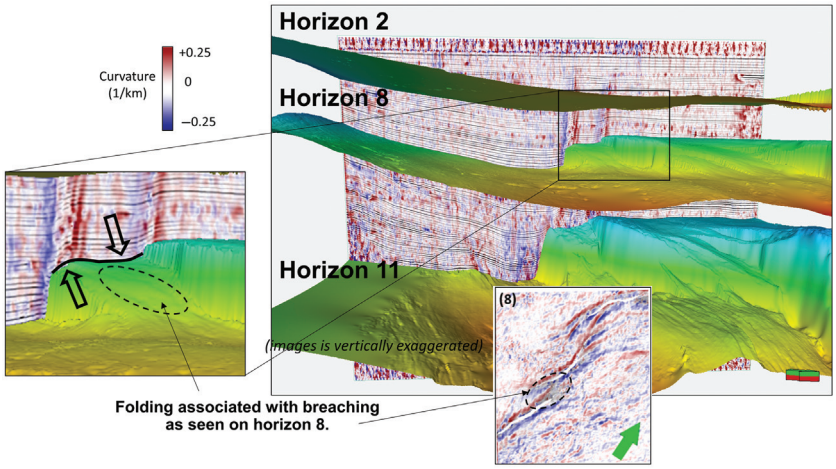

Figure 14. Time-structure maps of horizons 2, 8, and 11, and a vertical slice through the corendered most-positive curvature, k1, most-negative curvature, k2, and seismic amplitude, showing the correlation of positive-curvature anomalies with the hanging. Folding associated with breaching as shown on horizon 8 to be predominately an anticlinal shape (positive curvature) — due to possible twisting.

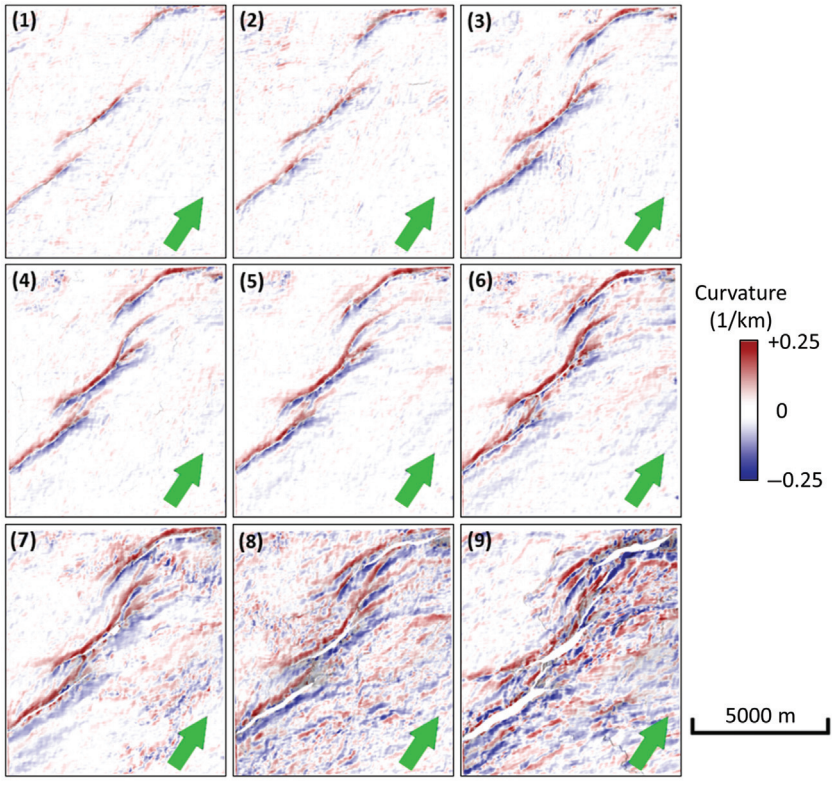

Figure 15. Corendered most-positive (k1) and most-negative (k2) curvatures computed from picked horizons 1 to 9 showing an increase in curvature associated with increased displacement.

Analysis

Understanding attributes

Based on the results presented above and the observation from the application of seismic attributes to faults and horizons, understanding the deformation mechanism and growth history of some of the transfer zones can be accomplished. By examining the seismic dip data, the bed dips can be imaged to determine the degree of deformation that transfer zones have undergone. As the displacement increases within the relay ramps, beds within the ramp rotate to accommodate the displacement. Above a certain dip angle, the ramps cannot further accommodate the additional displacement leading to the formation of smaller faults. This critical dip for the formation of secondary faults is likely controlled by the lithologic composition of the beds. This growth model approach is consistent with the model that Peacock and Sanderson (1994) suggest in which faulting is seen to occur postbreaching or splay formation. We see no evidence that transfer zones are breaching and rotation and fracturing of beds are occurring posthard-link faulting development.

The intensity of breaching experienced by ramp 1 and ramp 2 can be seen using the seismic dip data as well as the variance and curvature. This observation is consistent with the bed rotation deformation mechanism and indicates the higher density of fracturing with deeper formations/horizons that have undergone further deformation. Similarly, in Figure 14, the degree of curvature can be seen to correlate with the amount of displacement on the faults. As the displacement increases, the amount of curvature increases indicating the increased bed rotation. By examining the cross section shown in Figure 3, the overall geometry of the beds outside the fault zones is seen to

be flat, with consistent rotation near the fault. The magnitude of rotation and the width of the folded zone is associated with the displacement as well as the lithology. However, lithologic implications might have limited controlling factor to the degree of fracturing that those beds and ramps are showing compared with the displacement. Traditional models of transfer zones (such as the one suggested by Morley et al., 1990) show only broad rollover folding of beds related to the changes in fault dip, but no additional folding in the immediate vicinity of the fault. However, experimental studies (Paul and Mitra, 2013) suggest that, in many instances, additional extensional fault-propagation or drape folding occurs in the vicinity of the faults, altering the geometry of the transfer zone. Drape folds, accompanied by drag folding, produce the curvature changes described above for the Parihaka fault system. Therefore, the broader curvature changes directly record drape folding, whereas the sharp changes reflect the effects of the faulting. The presence of drape is also supported by the cross sections through the traditional amplitude data (Figure 3). Within the transfer zones, this indicates that many of those beds with maximum curvature observed indicates significant rotation and thus a higher amount of fracturing or faulting, which accompany the splay faults formation.

In addition, variance extracted along each of the fault planes shows a correlation with the calculated displacement that faults have undergone. This observation indicates that the similarity between the upthrown and downthrown blocks is significantly reduced for the deeper formation, hence hinting at significant changes in the seismic response. This is partially caused by the higher displacement and juxtaposition of different formations, and it is significantly related to the additional breaking and fracturing that fault zones experience. Despite it being hard to assess the degree of fracturing that damage zones have experienced, it can be qualitatively estimated that a higher degree of breaking is expected.

Work application and implications

The application of seismic attributes in hydrocarbon exploration provides a deeper understanding of the structural and stratigraphic elements of the system. When assessing the risk associated with transfer zones, in particular, an understanding of timing and degree of deformation are important. Through this work, the seismic dip proved to be a good approximation of the actual dip of the relay ramp and can highlight zones within ramps that might have undergone additional deformation and breaching. As was seen through our work, a 5° dip rotation is sufficient to cause breaching within ramps. Similarly, variance attributes can be used as a qualitative indicator of displacement experienced by faults. Because variance exhibits a logarithmic shape, it provides additional insights regarding fault splaying and breaching locations. Quantitative measurements of displacement are possible as well for a low degree of variance.

Understanding breaching locations and timing has significant implications in understanding hydrocarbon movement and storage. Depending on the time of expulsion of the hydrocarbon in the Taranaki Basin, those relay ramps could have served as pathways for hydrocarbon movement from the downthrown to the upthrown side. However, if breaching, as seen via seismic dip and variance, is associated with significant displacement and preceded expulsion of hydrocarbons, it is then possible that some of the compartments that formed around those faults are great reservoir targets. That will depend on the formation that the hydrocarbons migrated from and the one they migrated through. Hence, understanding the timing and degree of deformation is of the essence for hydrocarbon exploration.

In addition, the use of curvature does show possible folding and tilting of beds, which could serve as additional locations for hydrocarbon accumulations. Because displacement increases with curvature, curvature might be as well be used to indicate the location of high fracture density, which can be migration pathways for conventional reservoirs or a storage zone for unconventional exploration. Hence, seismic attributes can provide additional understanding on reservoir compartmentalization and the structural properties associated with the faults' movements.

When it comes to understanding the structural evolution of the Taranaki Basin and the Parihaka fault, the work presented here provides an additional understanding of the deformation of the region. As discussed earlier, the southern part of the Taranaki Basin has undergone significant deformation during the Pliocene. However, and during the Pleistocene, the maximum displacement on the faults is seen to be shifting toward the northern part of the basin, possibly associated with the rollback of the Pacific Plate and an increase in volcanic activity in the region.

Locally, it can be concluded that the en echelon faulting predefines the width of the transfer zones. The relay ramp width is seen to be related to the relative fault locations, whereas the fault length is associated with the fault displacement. As the displacement increases, the overlapping fault length increases causing a rotation in fault tips into the transfer zone. The evolution of the transfer zone and faulting of the ramp connection of each of two major faults is seen to be a function of the amount of displacement and the rotation of the beds. As breaching occurs, the fault growth appears to cease, thus causing the deformation to be transferred to smaller faults within the ramps. Hence, the deeper formations, having undergone significantly more displacement than the younger formations, are seen to be heavily faulted and fractured in areas around the transfer zones. Hence, the evolution of the Parihaka fault becomes more complex for hydrocarbon exploration.

Conclusion

The Parihaka fault system consists of a set of three en echelon faults trending northeast–southwest. The

DOI:10.1190/INT-2020-0138.1

displacement associated with these faults shows an increase along the southern part during the Pliocene and to the northern part during the Pleistocene. This change in displacement can be seen in the changes of bed thickness on the downthrown block and is possibly due to the rotation of the stress field.

The relay ramps connecting those faults indicate that the faults gained the bulk of their length with an initially small displacement. As the displacement increased, the ramp lengths increased, thus connecting the major faults and causing faults to rotate and terminate against each other. An additional increase in the displacement, beyond the early displacement, is shown not to translate into additional fault length increase. The width of the ramps is predefined by the original location of the faults. With additional displacement, beds within the ramps rotate approximately 6° causing the beds to break and form smaller faults to accommodate for the additional faulting. The development of the smaller faults can be seen using the seismic dip attributes.

Seismic attributes can improve the understanding of transfer zones' characteristics and derivation of structural properties. Coherence shows a positive correlation between variance and displacement. Below a certain variance value (0.6), displacement is consistent and can be calculated. This has important implications for smaller faults such as within the relay ramps and fault splays where variance can be used to detect fault displacement. Seismic curvature provides a good indication of the folding associated with the faulting. Positive curvature indicates anticlinal features, whereas negative curvature indicates synclinal features. The application of seismic attributes to structural interpretation of transfer zones can assist in better understanding the details of the structural geometry and history of the study area. Different attributes can detect faulting propagation, deformation transfer, bed rotation, and stress orientation. These features as well as the effects of lithologic variation on structural geometry can explain the variation in deformation styles in the fault system.

Acknowledgments

The authors would like to thank SEG for providing the data through the SEG Data Storage Facility, as well as the reviewers for their valued feedback and comments that greatly improved the manuscript. This work was made possible thanks to the support of Baker Hughes Inc. (JewelSuite), Devon Energy, the University of Oklahoma, Schlumberger (Petrel), and the AASPI consortium by providing the software and tools needed.

Data and materials availability

Data associated with this research are available and can be accessed via the following URL: https://wiki.seg.org/wiki/Open_data.

References

Bahorich, M., and S. Farmer, 1995, 3-D seismic discontinuity for faults and stratigraphic features: The coherence cube: The Leading Edge, **14**, 1053–1058, doi: 10.1190/1.1437077.

Conneally, J., C. Childs, and J. J. Walsh, 2014, Contrasting origins of breached relay zone geometries: Journal of Structural Geology, **58**, 59–68, doi: 10.1016/j.jsg.2013.10.010.

Ferrill, D. A., and A. P. Morris, 2008, Fault zone deformation controlled by carbonate mechanical stratigraphy, Balcones fault system, Texas: AAPG Bulletin, **92**, 359–380, doi: 10.1306/10290707066.

Fossen, H., and A. Rotevatn, 2016, Fault linkage and relay structures in extensional settings — A review: Earth-Science Reviews, **154**, 14–28, doi: 10.1016/j.earscirev.2015.11.014.

Gersztenkorn, A., and K. J. Marfurt, 1999, Eigenstructure-based coherence computations as an aid to 3-D structural and stratigraphic mapping: Geophysics, **64**, 1468–1479, doi: 10.1190/1.1444651.

Giba, M., A. Nicol, and J. J. Walsh, 2010, Evolution of faulting and volcanism in a back-arc basin and its implications for subduction processes: Tectonics, **29**, TC4020, doi: 10.1029/2009TC002634.

Giba, M., J. J. Walsh, and A. Nicol, 2012, Segmentation and growth of an obliquely reactivated normal fault: Journal of Structural Geology, **39**, 253–267, doi: 10.1016/j.jsg.2012.01.004.

Haque, A. E., M. A. Islam, and M. Ragab Shalaby, 2016, Structural modeling of the Maui Gas Field, Taranaki Basin, New Zealand: Petroleum Exploration and Development, **43**, 965–975, doi: 10.1016/S1876-3804(16)30114-8.

Iacopini, D., R. W. H. Butler, S. Purves, N. Mcardle, and N. De Freslon, 2016, Exploring the seismic expression of fault zones in 3D seismic volumes: Journal of Structural Geology, **89**, 54–73, doi: 10.1016/j.jsg.2016.05.005.

King, P. R., 2000, Tectonic reconstructions of New Zealand: 40 Ma to the Present: New Zealand Journal of Geology and Geophysics, **43**, 611–638, doi: 10.1080/00288306.2000.9514913.

King, P. R., and G. P. Thrasher, 1996, Cretaceous-Cenozoic geology and petroleum systems of the Taranaki Basin, New Zealand: Institute of Geological & Nuclear Sciences.

Larsen, P.-H., 1988, Relay structures in a Lower Permian basement-involved extension system, East Greenland: Journal of Structural Geology, **10**, 3–8, doi: 10.1016/0191-8141(88)90122-8.

Lohr, T., C. M. Krawczyk, O. Oncken, and D. C. Tanner, 2008, Evolution of a fault surface from 3D attribute analysis and displacement measurements: Journal of Structural Geology, **30**, 690–700, doi: 10.1016/j.jsg.2008.02.009.

Marfurt, K. J., 2006, Robust estimates of 3D reflector dip and azimuth: Geophysics, **71**, no. 4, P29–P40, doi: 10.1190/1.2213049.

Marfurt, K. J., 2010, The shape of seismic interpretation, *in* L. J. Wood, T. T. Simo, and N. C. Rosen, eds., Seismic imaging of depositional and geomorphic systems: Society of Economic Paleontologists and Mineralogists, 241–294.

Morley, C. K. R., A. Nelson, T. L. Patton, and S. G. Munn, 1990, Transfer zones in the East African Rift system and their relevance to hydrocarbon exploration in rifts: AAPG Bulletin, **74**, 1234–1253, doi: 10.1306/0C9B2475-1710-11D7-8645000102C1865D.

Nicol, A., C. Mazengarb, F. Chanier, G. Rait, C. Uruski, and L. Wallace, 2007, Tectonic evolution of the active Hikurangi subduction margin, New Zealand, since the Oligocene: Tectonics, **26**, TC4002, doi: 10.1029/2006TC002090.

Paul, D., and S. Mitra, 2013, Experimental models of transfer zones in rift systems: AAPG Bulletin, **97**, 759–780, doi: 10.1306/10161212105.

Peacock, D. C., and D. J. Sanderson, 1991, Displacements, segment linkage and relay ramps in normal fault zones: Journal of Structural Geology, **13**, 721–733, doi: 10.1016/0191-8141(91)90033-F.

Peacock, D. C. P., and D. J. Sanderson, 1993, Estimating strain from fault slip using a line sample: Journal of Structural Geology, **15**, 1513–1516, doi: 10.1016/0191-8141(93)90011-X.

Peacock, D. C. P., and D. J. Sanderson, 1994, Geometry and development of relay ramps in normal fault systems 1: AAPG Bulletin, **2**, 147–165, doi: 10.1306/BDFF9046-1718-11D7-8645000102C1865D.

Peacock, D. C. P., and D. J. Sanderson, 1995, Strike-slip relay ramps: Journal of Structural Geology, **17**, 1351–1360, doi: 10.1016/0191-8141(95)97303-W.

Rajabi, M., M. Ziegler, M. Tingay, O. Heidbach, and S. Reynolds, 2016, Contemporary tectonic stress pattern of the Taranaki Basin, New Zealand: Journal of Geophysical Research, Solid Earth, **121**, 6053–6070, doi: 10.1002/2016JB013178.

Reilly, C., A. Nicol, J. J. Walsh, and H. Seebeck, 2015, Evolution of faulting and plate boundary deformation in the Southern Taranaki Basin, New Zealand: Tectonophysics, **651–652**, 1–18, doi: 10.1016/j.tecto.2015.02.009.

Roberts, A., 2001, Curvature attributes and their application to 3D interpreted horizons: First Break, **19**, 85–100, doi: 10.1046/j.0263-5046.2001.00142.x.

Rotevatn, A., C. A.-L. Jackson, A. B. M. Tvedt, R. E. Bell, and I. Blækkan, 2018, How do normal faults grow?: Journal of Structural Geology, **125**, 174–184, doi: 10.1016/j.jsg.2018.08.005.

Stern, T. A., and W. E. Holt, 1994, Platform subsidence behind an active subduction zone: Nature, **368**, 233–236, doi: 10.1038/368233a0.

Thorsen, C. E., 1963, Age of growth faulting in southeast Louisiana: GCAGS Transactions, **13**, 103–110.

Tripathi, A. R. P., and P. J. J. Kamp, 2008, Timing of initiation of reverse displacement on the Taranaki Fault, northern Taranaki Basin: Constraints from the on land record: Oligocene Te Kuiti Group, 1–17.

Walsh, J. J., and J. Watterson, 1988, Analysis of the relationship between displacements and dimensions of faults: Journal of Structural Geology, **10**, 239–247, doi: 10.1016/0191-8141(88)90057-0.

Dr. Kurt J. Marfurt began his geophysical career teaching geophysics and contributing to an industry-supported consortium on migration, inversion, and scattering (project MIDAS) at Columbia University's Henry Krumb School of Mines in New York City. In 1981, he joined Amoco's Tulsa Research Center and spent the next 18 years doing or leading research efforts in modeling, migration, signal analysis, basin analysis, seismic attribute analysis, reflection tomography, seismic inversion, and multicomponent data analysis. In 1999, he joined the University of Houston as a professor in the Department of Geosciences and as director of the Allied Geophysics Laboratories. He is currently a member of the Geophysical Societies of Tulsa and Houston, SEG, EAGE, AAPG, AGU, and SIAM, and he serves as the deputy editor-in-chief of *Interpretation*. His current research activity includes prestack imaging, velocity analysis and inversion of converted waves, computer-assisted pattern recognition of geologic features on 3D seismic data, and interpreter driven seismic processing. His research interests include seismic signal analysis, 3D seismic attributes, seismic velocity analysis, subsurface imaging, and multicomponent data analysis.

Pierre Karam received a bachelor's degree in civil and environmental engineering from the Lebanese American University. He then received master's and doctoral degrees in geology from the University of Oklahoma. He is currently working as a geoscientist at Devon Energy in Oklahoma City focusing on subsurface modeling.